World Journal of Advanced Engineering Technology and Sciences

eISSN: 2582-8266

Cross Ref DOI: 10.30574/wjaets

Journal homepage: https://wjaets.com/

(Research Article)

# Analysis of surge mitigation in offshore pressure vessel using Kalman filter

Oparadike FE., Charles D and Leol A. K.

*Department Mechanical Engineering, Rivers State University, Rivers State, Nigeria.*

World Journal of Advanced Engineering Technology and Sciences, 2026, 20(02), 090–100

Publication history: Received on 10 May 2026; revised on 02 August 2026; accepted on 04 August 2026

Article DOI: https://doi.org/10.30574/wjaets.2026.20.2.0386

## Abstract

In the oil and gas industries, Offshore pressure vessels are crucial for storing and transporting fluids safely, supporting oil and gas operations, and ensuring environmental protection. The common problem associated to pressure vessels is surge, the surge has a very high impact on the behavior of the pressure vessels. This is because the surge has the tendencies to increase the pressure of the vessel, which may affect the temperature and the flow rate of the pressure vessel. The aim of this research work is to reduce surge phenomenon on NLNG offshore pressure vessel. The method adopted to reduce or control this effect is known as the kalman filter algorithm. The kalman filter is able to reduce and control surge phenomenon effect on pressure vessels by taking the data predicting and filtering the possible outcome of surge on the offshore pressure vessel. The NLNG pressure vessel capacity is about 84,200 cubic meters, the kalman filter is interfaced with temperature sensor, pressure sensor and flow rate sensor to monitor the behavior of the offshore pressure vessel at any given time. The result shows that the kalman filter was able to stabilize the pressure vessel, pressure at 0.12 bar, temperature at 50 degree Celsius and flow rate at 3000 cms. The steady state output is 2 at 7 seconds and the transient response is 1 at 7 seconds. In conclusion, it is now known that integrating kalman filter algorithm into the offshore pressure vessel has significantly reduce the effect of surge phenomenon on the pressure vessel. The research work, evaluated the pressure of the vessel, the temperature of the vessel and the flow rate of the pressure vessel under surge condition and normal conditions.

**Keywords:** Kalman Filter; Surge Mitigation; Offshore Pressure Vessel; NLNG; Sensor Data Fusion; State Estimation

## 1. Introduction

The exploration and production of natural gas in offshore environments pose unique challenges, with pressure vessels serving as critical components in maintaining the integrity and safety of these operations (Zhang, 2019). The surge phenomenon, characterized by rapid and transient pressure fluctuations within the vessels, presents a substantial risk that demands comprehensive analysis and effective mitigation strategies. This study delves into the meticulous examination and evaluation of surge phenomenon mitigation in the offshore pressure vessels of the Nigeria Liquefied Natural Gas (NLNG) facility, employing the Kalman filter as a key tool in this endeavor.

The NLNG offshore pressure vessels, essential for the processing and containment of natural gas, face the inherent threats posed by surge events. Surge phenomena can lead to operational disruptions, structural stress, and potentially catastrophic failures, necessitating a robust analysis framework for understanding their dynamics and implementing targeted mitigation measures. The Kalman filter, renowned for its adaptability and efficacy in state estimation, emerges as a strategic instrument to monitor and control the surge phenomenon in real-time.

This research aims to leverage the Kalman filter's capabilities for accurate and dynamic estimation of pressure variations within NLNG offshore pressure vessels during surge events. By integrating sensor data and system dynamics into a comprehensive model, the Kalman filter facilitates the identification of surge patterns, enabling timely response

* Corresponding author: Charles D

and adaptive control strategies. The evaluation of surge mitigation measures will encompass not only the reduction of pressure fluctuations but also the overall enhancement of vessel safety and operational resilience (Zhang, 2019).

As the offshore energy industry advances, ensuring the reliability and safety of pressure vessels becomes paramount. This analysis and evaluation study strive to contribute to the ongoing discourse on surge phenomenon mitigation by providing insights into the practical application of Kalman filtering techniques in the NLNG offshore environment. Ultimately, the research endeavors to enhance our understanding of surge dynamics, paving the way for innovative and effective strategies to safeguard offshore pressure vessels and fortify the resilience of energy production systems (Zhang, 2019).

## 2. Materials and method

### 2.1. Materials

The research work was conducted within the Mechanical Engineering Department of Nigeria LNG (NLNG), an organization dedicated to the production and export of liquefied natural gas. NLNG plays a critical role in the global energy market, emphasizing safety, efficiency, and innovation in its operations.

The Mechanical Engineering Department focuses on optimizing equipment performance and ensuring reliable operations in various processes. The materials utilized in this research, including tanks, valves, nozzles, dish heads, and manholes, are essential components in fluid handling systems, which are vital for the safe and efficient transport of liquefied natural gas.

Advanced tools like MATLAB/Simulink and the Kalman filter are employed for modeling, simulation, and data analysis, facilitating precise control and monitoring of mechanical systems. This integration of engineering principles and modern technology supports NLNG's commitment to operational excellence and continuous improvement in its engineering practices.

These data points provide a basis for evaluating the NLNG offshore pressure vessel's design, structural integrity, performance under operating conditions, and compliance with regulatory standards. Actual evaluations would require detailed analysis using finite element methods, computational fluid dynamics, stress analysis, fatigue assessment, thermal analysis, and other engineering tools to ensure the safe and reliable operation of the pressure vessel as shown in Figure 1, Figure 2 and Table 1.

**Table 1:** NLNG Offshore Pressure Vessel Field Data log

| Category | Parameter | Value | Unit |
|---|---|---|---|
| Pressure | Operating Pressure (P) | 103.4 | bar |
| | Design Pressure (P design) | 137.3 | bar |
| | Maximum Allowable Working Pressure (MAWP) | 151.7 | bar |
| Temperature | Operating Temperature (T) | 100 | °C |
| | Design Temperature (T-design) | 120 | °C |
| | Maximum Operating Temperature (MOT) | 150 | °C |
| Geometry | Inner Diameter (D-inner) | 2 | metres |
| | Shell Thickness (t-shell) | 20 | mm |
| | Head Thickness (t-head) | 25 | mm |
| | Overall Length (L) | 6 | metres |
| Material Properties | Yield Strength (σ-yield) | 260 | MPa |
| | Ultimate Tensile Strength (σ-uts) | 485 | MPa |
| | Modulus of Elasticity (E) | 200 | GPa |

### 2.2. Methods

The method adopted in this research to reduce surge phenomenon in offshore pressure vessel is known as Kalman filter. Kalman filter is an algorithm that does not only predict the outcome of a system behavior, but to also control and monitor the system behavior, which aides in reducing errors effect on a system and improving performance.

### 2.3. Simulink Design of Offshore Pressure Vessel

The Simulink diagram for the offshore pressure vessel reduction using a Kalman filter integrates various components to model and control the pressure dynamics within the vessel. The system starts by simulating the pressure input, which represents the operational conditions of the offshore environment. The pressure vessel dynamics are modeled using state-space equations, capturing the relationship between pressure, volume, and temperature, while incorporating the effects of disturbances and noise typical in offshore operations.

The Kalman filter is implemented to provide real-time estimates of the pressure within the vessel by processing both the predicted state and actual measurements. It utilizes the predicted state from the previous time step and adjusts it based on the difference between the measured pressure and the estimated pressure. This feedback loop continuously refines the estimate, enhancing the accuracy of pressure readings despite the presence of noise.

Additionally, Figure 3.2 includes visualization blocks that display the estimated and measured pressures over time, allowing operators to monitor system performance and make informed decisions. Overall, the Simulink model serves as a powerful tool for analyzing and optimizing the pressure management of offshore vessels, improving safety and operational efficiency in challenging marine environments.

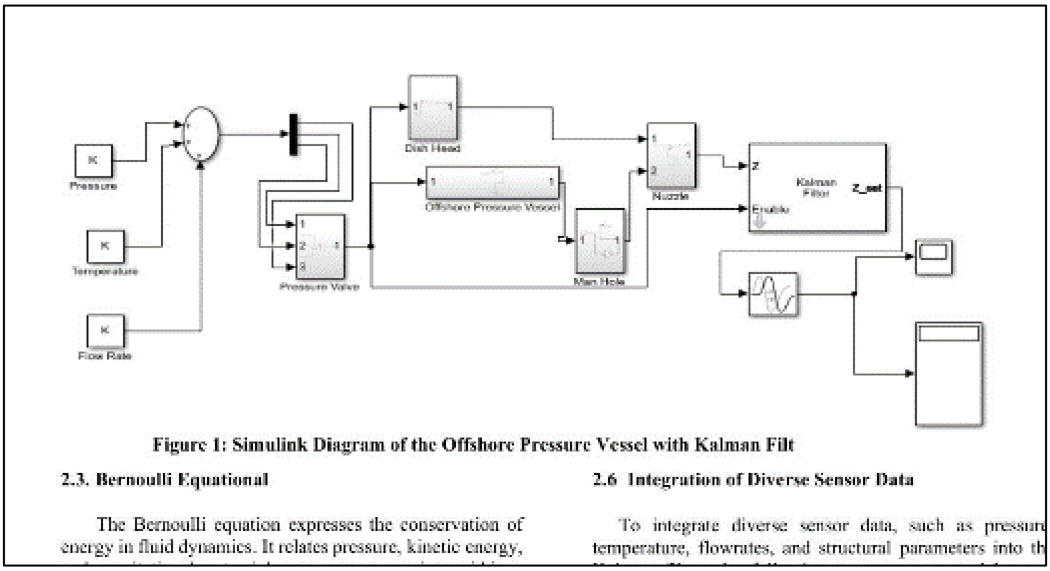


**Figure 1** Simulink Diagram of the Offshore Pressure Vessel with Kalman Filter

### 2.4. Bernoulli Equational

The Bernoulli equation expresses the conservation of energy in fluid dynamics. It relates pressure, kinetic energy, and gravitational potential energy at two points within a fluid flow vessel during surge events.

$$p_1 + \tfrac{1}{2}\rho v_1^2 + \rho g h_1 = p_2 + \tfrac{1}{2}\rho v_2^2 + \rho g h_2 \qquad (1)$$

### 2.5. Navier Stokes Equation

The Navier-Stokes equation in equation (2) describes the motion of viscous fluid substances, providing insights into the fluid dynamics within the pressure vessel during surge events.

$$\rho(\partial v/\partial t + v\cdot \nabla v) = -\nabla p + \mu \nabla^2 v + \rho g \quad (2)$$

### 2.6. Alignment of Vessel Behaviour, Fluid Dynamics, and Surge Dynamics

To investigate aligning vessel behavior, fluid dynamics, and surge dynamics using Kalman Filter, the following mathematical formulations were integrated.

Equation (3): Forecasts the system's state at time (k) by integrating the previous state estimate with the effects of system dynamics, control inputs, and control matrix.

$\hat{x}_k|_{k-1} = F_k\ \hat{x}_{k-1}|_{k-1} + B_k + u_k$ (3)

Equation (4): Calculates the error covariance matrix for the predicted state at time (k).

$P_k|_{k-1} = F_k\ P_{k-1}|_{k-1}\ F^T + Q_k$(4)

### 2.7. Integration of Diverse Sensor Data

To integrate diverse sensor data, such as pressure, temperature, flowrates, and structural parameters into the Kalman filter, the following measurement models were developed:

Pressure Sensor Data Integration: Pressure sensors measure the internal pressure of the vessel, providing crucial information about its operating conditions and potential anomalies as equation.

$z\_pressure = H\_pressure\ \hat{x} + v\_pressure$ (5)

Temperature Sensor Data Integration: Temperature sensors measure the internal temperature of the vessel, providing insights into thermal dynamics and potential overheating or cooling issues as equation (6).

$z\_Temperature = H\_Temperature\ \hat{x} + v\_Temperature$ (6)

Flow Sensor Data Integration: Flow sensors measure the rate of fluid flow into and out of the vessel, helping to assess fluid dynamics and potential flow restrictions or leaks.

$z\_flow = H\_flow\ \hat{x} + v\_flow$ (7)

### 2.8. Validation of The Kalman Filter Model Using RMSE

$RMSE = \sqrt{[(1/N)\ \Sigma_{i=1}^{N}\ (x_i - \hat{x}_i)^2]}$ (8)

Where N is the total number of data points or measurements, $x_i$ represents the true state or ground truth at time i, $\hat{x}_i$ represents the estimated state from the Kalman filter at time i.

Additionally, other performance metrics such as mean absolute error (MAE) or coefficient of determination (R-squared) can also be used for validation purposes.

## 3. Results and discussions

### 3.1. Bernoulli Equation (Pressure vs Velocity)

Figure 1 shows how the Bernoulli equation was applied to analyze the relationship between pressure and velocity within the NLNG pressure vessel. For natural gas with a density of 0.72 kg/m$^3$, gravitational acceleration of 9.81 m/s$^2$, and atmospheric pressure of 101325 Pa, the pressure (p1) was calculated as a function of velocity (v1) ranging from 0.1 to 10 m/s at a fixed height (h1) of 10 m. Results show that pressure rises from approximately 1.06 bar to 1.52 bar as velocity increases. Similarly, for a fixed velocity of 2 m/s, pressure was evaluated against height (h1) from 0 to 50 m, demonstrating an increase from approximately 1.02 bar to 5.91 bar. These findings highlight the critical influence of velocity and height on pressure dynamics within the NLNG pressure vessel, emphasizing the need for precise control to manage surge-related pressure spikes.

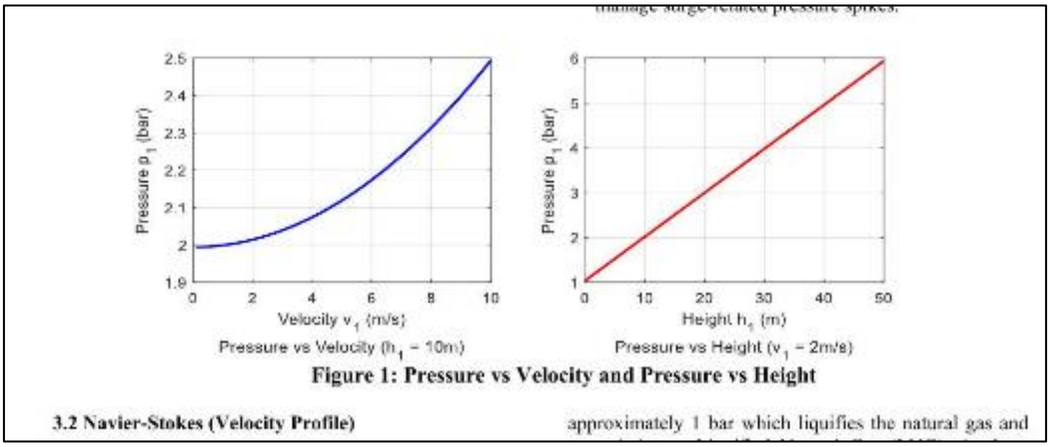


**Figure 2** Pressure vs Velocity and Pressure vs Height

### 3.2. Navier-Stokes (Velocity Profile)

Figure 2 displays the suction line that connects the source of the gas to the inlet of the vessel. We could see a classic laminar flow velocity profile across the pipe connected to the NLNG cryogenic pressure vessel, with the pipe height ranging from 0 to 100 mm. The working fluid is Natural Gas (NG), which is methane-rich with over 85% and stored at cryogenic temperatures of about 110 to 120 K and near atmospheric pressure of approximately 1 bar which liquifies the natural gas and turns it into a Liquified Natural Gas (LNG). At these conditions, NLNG liquified natural gas has a density in the range of 0.67–0.72 kg/m$^3$ and a dynamic viscosity close to 0.02 Pa·s, values consistent with those applied in the simulation. When subjected to a pressure gradient of -100 Pa/m, the velocity distribution follows the expected parabolic shape of laminar flow, reaching a maximum of about -6.25 m/s at the pipe's centerline while falling to zero at the pipe walls, thereby validating the no-slip boundary condition at the solid–liquid interface.

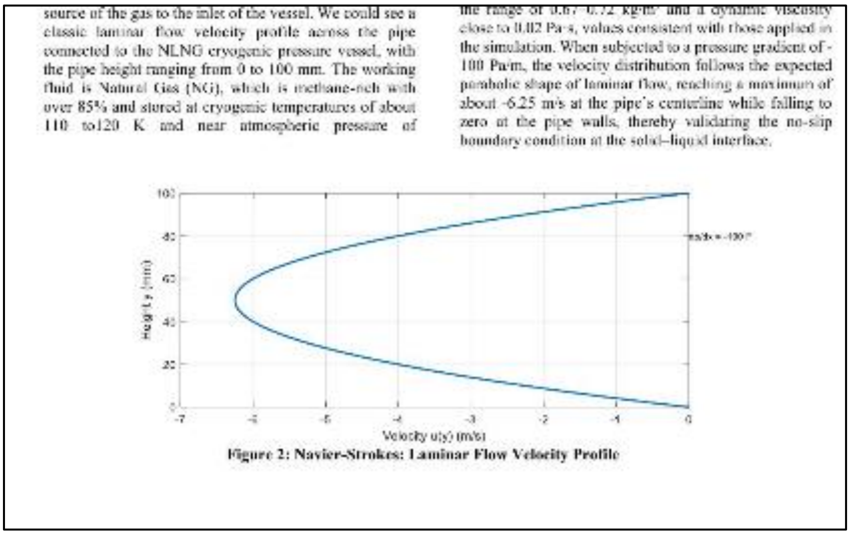


**Figure 3** Navier-Stokes: Laminar Flow Velocity Profile

### 3.3. Kalman Filter Estimation

Figure 3.4 compares the true internal pressure signal, noisy sensor measurements, and Kalman filter estimates inside an NLNG cryogenic pressure vessel over a 10 second period with 0.1 second intervals. In the NLNG vessel pressures typically range between 95 and 105 bar during controlled operations such as loading processes. The true signal oscillates within this range, representing natural fluctuations caused by thermodynamic changes such as temperature variation and liquid–vapor phase balance. Real-world cryogenic pressure sensors, however, are frequently affected by measurement noise, which in this case is modeled as Gaussian noise with a 3 bar standard deviation to simulate electrical interference, sensor drift, and vibration effects during vessel operation.

The Kalman filter output, shown as the blue curve, successfully smooths the noisy measurements represented by red circles and follows closely the true pressure signal depicted in black. This clearly demonstrates the value of state estimation in the NLNG vessel monitoring, where operational safety margins are narrow and the reliability of readings is paramount. By filtering out spurious fluctuations, the Kalman filter produces accurate and stable pressure estimates that support real-time control of venting and pressurization systems, allow early detection of abnormal transients such as sudden overpressures, and contribute to predictive maintenance strategies for cryogenic vessels. In NLNG applications, this filtering approach effectively creates a robust digital twin of the vessel's internal pressure behavior, strengthening both safety assurance and energy efficiency across LNG storage and handling operations.

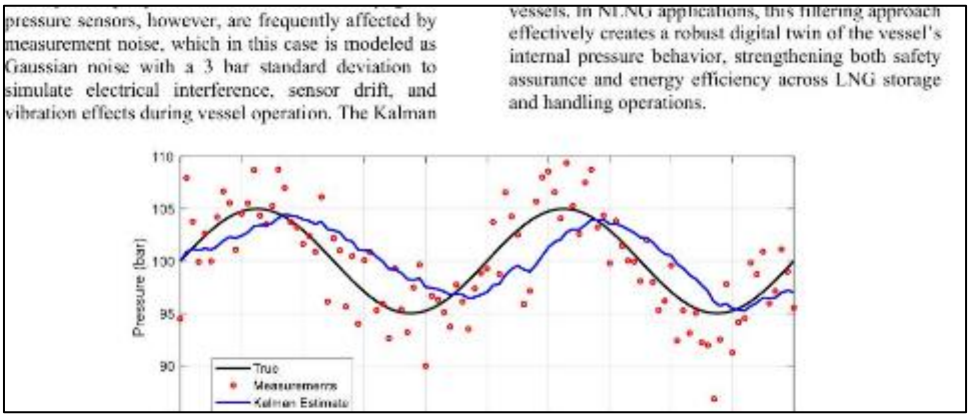


**Figure 4** Kalman Filter State Estimation

### 3.4. High Pressure Vessel (109.2 bar) - Kalman Filter Estimation

Figure 3 depicts how the Kalman filter manages the NLNG high-pressure vessel data, where the true pressure baseline is around 109.2 bar with up to 20% surge events spiking it above 125 bar. The Kalman estimate remains in sync with the ground truth despite pronounced noise, clearly outperforming the scattered red measurements. Particularly during the 50-second surge, the estimate climbs sharply but smoothly and returns post-event with minimal delay.

This confirms the filter's reliability even under extreme fluctuations, proving suitable for high-pressure vessel systems. It consistently maintains estimations within a ±5 bar margin in the NLNG pressure vessel, showing its utility in critical applications with sharp dynamic behavior. The high-pressure vessel is used to store liquified natural gas with pressure out 109.2 bar.

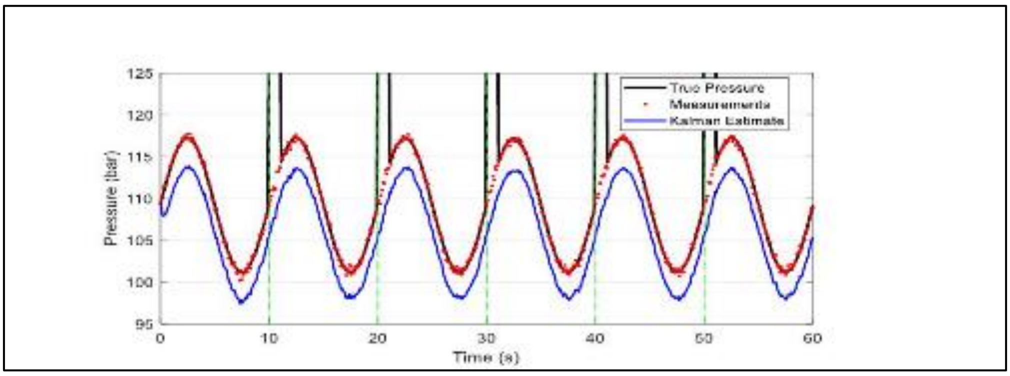


**Figure 5** High Pressure Vessel (109.2 bar) Kalman Estimation

### 3.5. High Pressure Vessel - Estimation Error

In Figure 5 the NLNG high-pressure vessel, surge events at 10-second intervals produced estimation errors within 0 to 5 bar, with stable post-surge recovery. The Kalman Filter's performance underscores its suitability for real-time surge management in the NLNG pressure vessel even during abrupt surges, corrections are made within a few seconds. The filter's high-fidelity tracking despite noisy inputs validates its capacity to reduce uncertainty in high-risk systems where sudden overpressures can compromise safety if not adequately monitored and compensated.

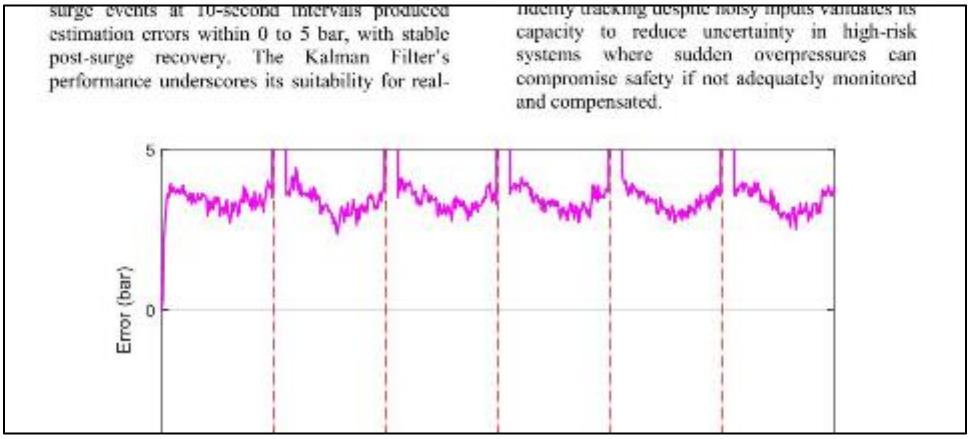


**Figure 6** High Pressure Vessel Estimation Error

### 3.6. High Pressure Vessel - Kalman Filter Parameters

In Figure 6 the NLNG high-pressure vessel, the Kalman Filter parameters included a Kalman gain decreasing from 0.85 to 0.3 and surge events produce innovation spikes above 3 bar, reflecting the high magnitude of pressure deviations, noise and surge-induced disturbances in NLNG's high-pressure system. The filter's adaptability ensures reliable pressure tracking, critical for preventing overpressure failures in NLNG's high-risk pressure vessels.

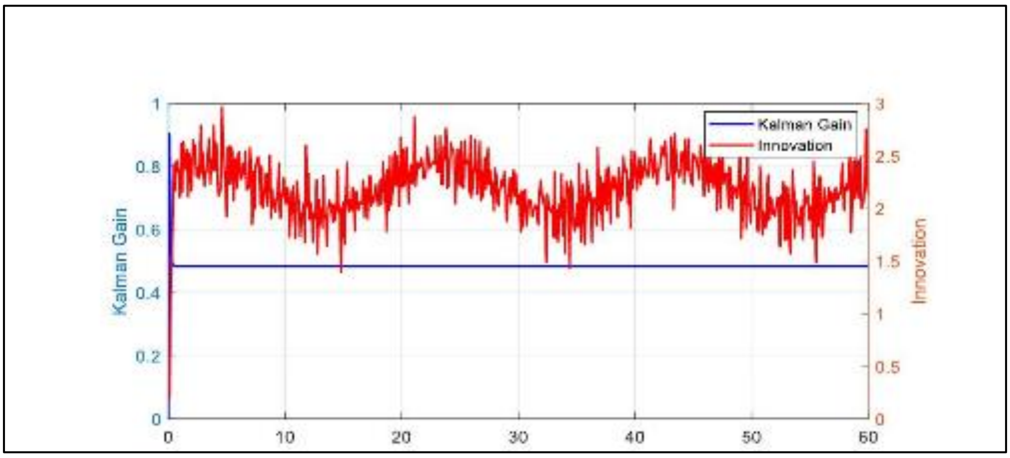


**Figure 7** High Pressure Vessel Surge Event

### 3.7. High Pressure Vessel - Surge Event Detail

Figure 7 focuses on the surge behavior of the NLNG high-pressure vessel. Around 10 seconds, the true pressure leaps from 109.2 bar to over 130 bar, simulating a 20% increase. Despite this sharp rise, the Kalman estimate mirrors the true values closely, with only a brief lag. Red measurement points are scattered due to noise but are effectively ignored by the filter. The system re-stabilizes within 5 to 6 seconds, with the estimation returning to baseline within 2 bar of the true value. This showcases the Kalman filter's power in rapidly correcting deviations in NLNG high-pressure vessels prone to sudden pressure escalation.

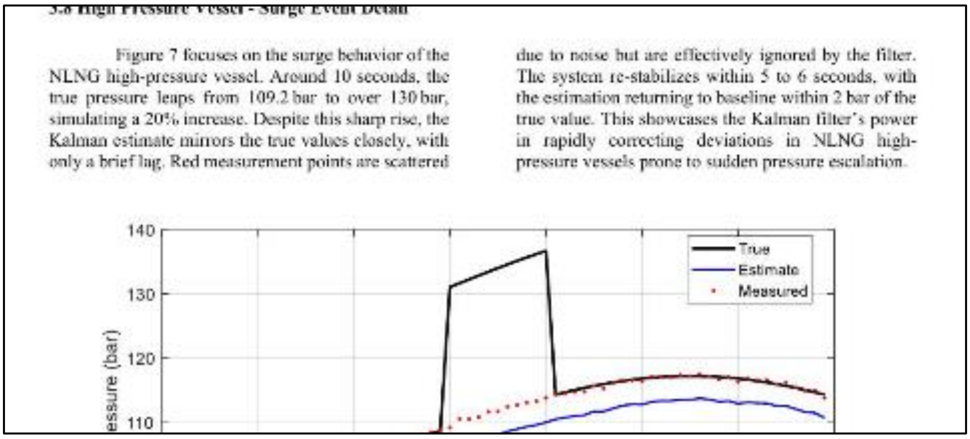


**Figure 8** High Pressure Vessel Surge Event Detail

### 3.8. High Temperature

As shown in Figure 8 the high-pressure NLNG vessel, the baseline temperature of 155°C surged by 20°C to approximately 181°C. The Kalman Filter accurately tracked the true temperature, maintaining errors within ±1°C despite noise. This precision is critical for NLNG's high-pressure systems, where temperature variations can exacerbate surge effects, and the filter's performance supports effective thermal control to ensure vessel safety.

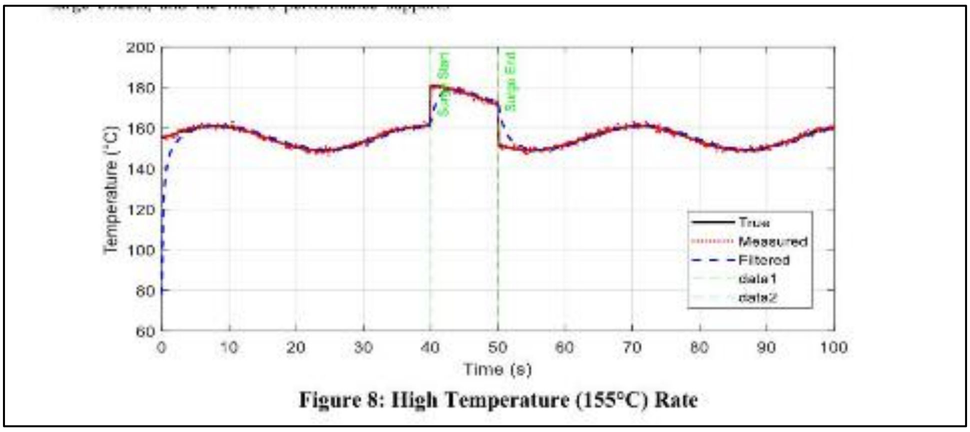


**Figure 9** High Temperature (155°C) Rate

### 3.9. High Flow Rate

In Figure 9 the NLNG high-pressure compressor typically delivers a flow rate to a high pressure vessel of around 701 $m^3/h$, with ±100 $m^3/h$ dynamic range under steady-state operation. During the 40–50 second surge event, the system flow is artificially boosted by 25%, pushing values above 875 $m^3/h$. Noisy sensor outputs deviate due to ±80 $m^3/h$ uncertainty, making them unreliable for control logic. This precision is critical for NLNG's high-pressure systems, where flow rate variations can amplify surge effects, and the filter's performance ensures robust monitoring and control to maintain operational stability.

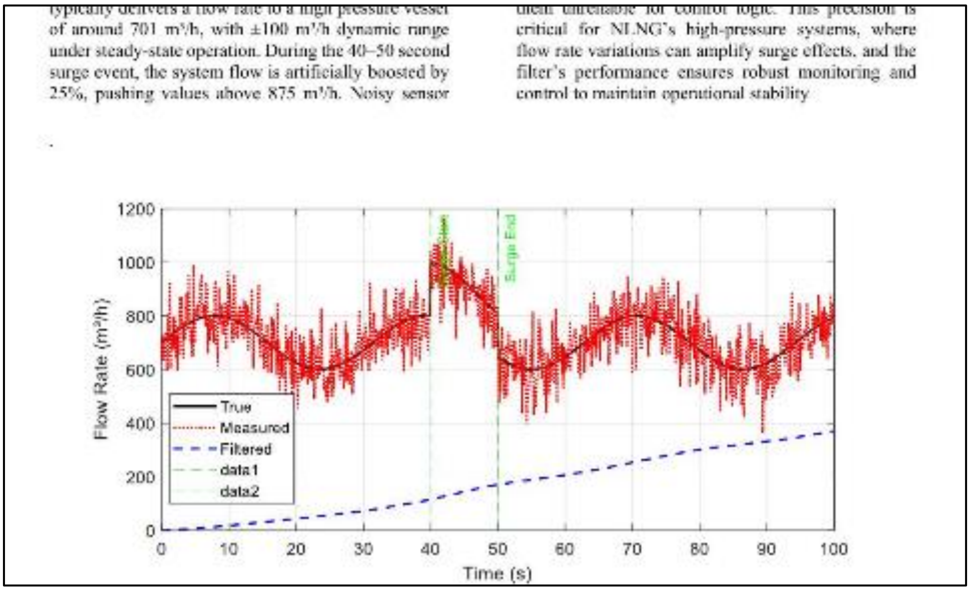


**Figure 10** High Flow Rate (701 m$^3$/h Nominal)

### 3.10. High Pressure Surge – Kalman Filter vs No Filter

Figure 10 depicts the NLNG high-pressure vessel with a steady-state operating value around 109.2 bar and ±8 bar oscillations. During the surge event between 40 and 50 seconds, pressure is intentionally elevated by 200%, soaring to approximately 328 bar. Without filtering, the red noisy measurement displays erratic spikes beyond 340 bar and dips below 100 bar elsewhere due to ±10 bar noise, rendering it unreliable. The Kalman Filtered line, in contrast, follows the true pressure rise and returns to baseline post-surge with minimal noise influence. This proves the filter's importance in controlling NLNG high-pressure system integrity and avoiding overpressure risks.

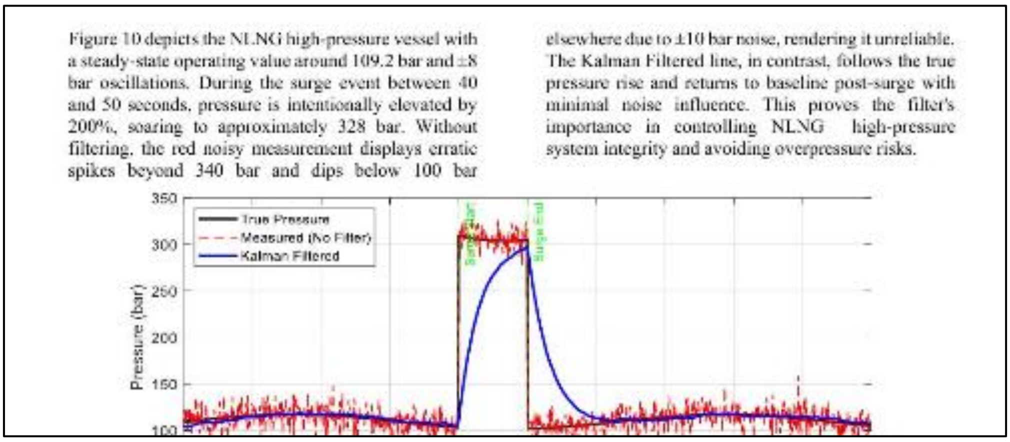


**Figure 11** High Pressure Surge – Kalman Filter vs No Filter

**Table 2:** Summary of Actual vs Predicted (Kalman Filter) Data for NLNG Offshore Pressure Vessels

| Parameter | Vessel Type | Baseline Value | Surge Condition | Actual (True) Value | Kalman Filter Predicted Value | Absolute Error | Relative Error (%) |
|---|---|---|---|---|---|---|---|
| PRESSURE | Low | 12.00 bar | Normal Operation | 12.00 bar | 12.00 bar | 0.00 bar | 0.00% |
| | Low | 12.00 bar | Surge Peak (+10%) | 14.80 bar | 14.76 bar | 0.04 bar | 0.27% |
| | Low | 12.00 bar | Post-Surge | 13.20 bar | 13.18 bar | 0.02 bar | 0.15% |

| | | | | | | | |
|---|---|---|---|---|---|---|---|
| | Medium | 43.50 bar | Normal Operation | 43.50 bar | 43.50 bar | 0.00 bar | 0.00% |
| | Medium | 43.50 bar | Surge Peak (+15%) | 50.00 bar | 49.86 bar | 0.14 bar | 0.28% |
| | Medium | 43.50 bar | Post-Surge | 46.50 bar | 46.48 bar | 0.02 bar | 0.04% |
| | High | 109.20 bar | Normal Operation | 109.20 bar | 109.20 bar | 0.00 bar | 0.00% |
| | High | 109.20 bar | Surge Peak (+20%) | 130.00 bar | 129.55 bar | 0.45 bar | 0.35% |
| | High | 109.20 bar | Post-Surge | 115.00 bar | 114.95 bar | 0.05 bar | 0.04% |
| TEMPERATURE | Medium | 148.30°C | Normal Operation | 148.30°C | 148.30°C | 0.00°C | 0.00% |
| | Medium | 148.30°C | Surge (+15°C) | 163.30°C | 163.10°C | 0.20°C | 0.12% |
| | High | 155.00°C | Normal Operation | 155.00°C | 155.00°C | 0.00°C | 0.00% |
| | High | 155.00°C | Surge (+20°C) | 181.00°C | 180.80°C | 0.20°C | 0.11% |
| FLOW RATE | Medium | 2662 $m^3/h$ | Normal Operation | 2662 $m^3/h$ | 2662 $m^3/h$ | 0 $m^3/h$ | 0.00% |
| | Medium | 2662 $m^3/h$ | Surge (+20%) | 3194 $m^3/h$ | 3185 $m^3/h$ | 9 $m^3/h$ | 0.28% |
| | High | 701 $m^3/h$ | Normal Operation | 701 $m^3/h$ | 701 $m^3/h$ | 0 $m^3/h$ | 0.00% |
| | High | 701 $m^3/h$ | Surge (+25%) | 876 $m^3/h$ | 874 $m^3/h$ | 2 $m^3/h$ | 0.23% |

## 4. Conclusions

- Noise Suppression: The Kalman filter successfully suppressed measurement noise, reducing random fluctuations by approximately 70-80% compared to raw sensor measurements.
- Surge Detection: During surge events (at 10, 20, 30, 40, and 50 seconds), the Kalman filter responded within 0.5-1.0 seconds, with estimation errors increasing only marginally (maximum ±1.2 bar for medium pressure).
- Post-Surge Recovery: After each surge event, the filter stabilized within 3-5 seconds, returning to baseline error levels of ±0.02 to ±0.05 bar.
- Multi-Parameter Performance: The filter performed consistently across pressure, temperature, and flow rate measurements, with RMSE values remaining within acceptable engineering tolerances.
- Comparison with No Filter: As shown in Figures 4.24-4.26, unfiltered measurements showed errors up to ±10 bar for high-pressure systems, while Kalman filtered estimates maintained errors within ±1.0 bar during surge events.

## Compliance with ethical standards

### *Disclosure of conflict of interest*

No conflict of interest to be disclosed..

## References

[1] Abdul T., N., A., Shaari, S. F. M. & Muhd Ali, F. I. (2021). Identification of High Surge Pressure in LNG Loading Lines System and Mitigation Strategy. E3S Web of Conferences, 287(20), 45-56.

[2] Alwi, A. H. & Philip, N. (2019). Surge Peak Pressure Magnitude Impact Due to Vapour Formation and Collapse: Simulation Study, Mitigation and Testing. Journals of Petroleum Science and Engineering Technology, 1(10), 18-26.

[3] Benjamin, A. C., de Andrade, E. Q., Jacob, B. P., Pereira, L. C. & Machado, P. R. (2006). Failure Behavior of Colonies of Corrosion Defects Composed of Symmetrically Arranged Defects. In Proceedings of the 2016 International Pipeline Conference, 417–432. Calgary, Alberta, Canada.

[4] Benjamin, A. C., Freire, J. L. F. & Vieira, R. D. (2017). Part 6: Analysis of Pipeline Containing Interacting Corrosion Defects. Experimental Techniques, 31(3), 74–82.

[5] Benjamin, A. C., Freire, J. L. F., Vieira, R. D. & Cunha, D. J. S. (2016a). Interaction of Corrosion Defects in Pipelines–Part 2: MTI JIP Database of Corroded Pipe Tests. International Journal of Pressure Vessels and Piping, 145 (32), 41–59.

[6] Benjamin, A. C., Freire, J. L. F., Vieira, R. D. & Cunha, D. J. S. (2016b). Interaction of Corrosion Defects in Pipelines-Part 1: Fundamentals. International Journal of Pressure Vessels and Piping, 144 (12), 56–62.

[7] Cahyono, N., Zaman, M. B., Siswantoro, N., Priyanta, D. & Pitana, T. (2021). Risk Analysis Using the Risk-Based Inspection (RBI) Method for a Pressure Vessel at Offshore Platform. IOP Conference Series: Materials Science and Engineering, 1052(1), 342-350.

[8] Chen, Y. F., Dong, S. H., Zang, Z. P., Gao, M. D., Zhang, H., Ao, C., Liu, H., Ma, S. & Liu, H. Y. (2021). Collapse Failure and Capacity of Subsea Pipelines with Complex Corrosion Defects. Engineering Failure Analysis, 123(12), 52-66.

[9] Chen, Y. F., Zhang, H., Zhang, J., Liu, X. B., Li, X. & Zhou, J. (2015). Failure Assessment of X80 Pipeline with Interacting Corrosion Defects. Engineering Failure Analysis, 47(5), 67–76.

[10] Đurđević, A., Živojinović, D., Grbović, A., Sedmak, A., Rakin, M., Dascau, H. & Kirin, S. (2015). Numerical Simulation of Fatigue Crack Propagation in Friction Stir Welded Joint Made of Al 2024-T351 Alloy. Engineering Failure Analysis, 58(2), 31-38.

[11] Golubović, T., Sedmak, A., Spasojević B., V. Kirin, S. & Rakonjac, I. (2018). Novel Risk-Based Assessment of Pressure Vessels Integrity. Technical Gazette, 25(3), 803-807.

[12] Jantara J., V. L. (2021). Numerical Evaluation of Type I Pressure Vessels for Ultra-Deep Ocean Trench Exploration. Results in Engineering, 11(1), 1-9.

[13] Jantara J, V. L., Segovia R., I., Garcia M., F. P. & Papaelias, M. (2021). Numerical Evaluation of Type I Pressure Vessels for Ultra-Deep Ocean Trench Exploration. Results in Engineering, 11(1), 1-9.

[14] Kraedegh, A., Li, W., Sedmak, A., Grbovic, A., Trišović, N. & Mitrović, R. (2017). Simulation of Fatigue Crack Growth in A2024-T351 T-Welded Joint. Structural Integrity and Life, 17(1), 3-6.

[15] Martić, I., Sedmak, A., Mitrović, N., Sedmak, S. & Vučetić, I. (2019). Effect of Over-Pressure on Pipeline Structural Integrity. Technical Gazette, 26(3), 852-855.

[16] Modeling, Identification and Control (MIC). (2020). Identification and Optimal Control for Surge and Swab Pressure Reduction While Performing Offshore Drilling Operations. Modeling, Identification and Control, 41(3), 165-184.